Clinical Neurophysiology 123 (2012) 2064–2073

Contents lists available at SciVerse ScienceDirect

Clinical Neurophysiology

journal homepage: www.elsevier.com/locate/clinph

# Are high-frequency (600 Hz) oscillations in human somatosensory evoked potentials due to phase-resetting phenomena?

Gunnar Waterstraat [a,*], Bartosz Telenczuk [a,b], Martin Burghoff [c,d], Tommaso Fedele [a,c,d], Hans J. Scheer [c,d], Gabriel Curio [a,d]

[a] Neurophysics Group, Department of Neurology, Campus Benjamin Franklin, Charite-University Medicine Berlin, Berlin, Germany
[b] Institute for Theoretical Biology, Humboldt-University Berlin, Berlin, Germany
[c] Physikalisch-Technische Bundesanstalt, Abbestr. 2-12, 10587 Berlin, Germany
[d] Bernstein Focus Neurotechnology, Berlin Institute of Technology, Chair Machine Learning, Fakultät IV, FR6-9, 10587 Berlin, Germany

ARTICLE INFO

*Article history:*
Accepted 24 March 2012
Available online 24 May 2012

*Keywords:*
Evoked potentials
High-frequency oscillations
Single-trial analysis
Phase-reset
Added-activity
Detectability analysis

HIGHLIGHTS

- Scalp recordings at an unprecedented low noise level show that high-frequency somatosensory evoked potentials (hfSEP) are generated by added-activity and not by a phase-reset of ongoing hf-activity as previously suggested.
- These seemingly contradictory results were reconciled by a statistical power analysis identifying the band-limited signal-to-noise ratio as decisive factor for the detectability of single-trial hfSEP added-activity.
- Thus, human scalp hfSEP can be understood as a non-invasively recorded correlate of evoked cortical multi-unit spike responses as inferred from previous invasive recordings.

ABSTRACT

*Objective:* Median nerve somatosensory evoked potentials (SEP) contain a brief oscillatory wavelet burst at about 600 Hz (σ-burst) superimposed on the initial cortical component (N20). While invasive single-cell recordings suggested that this burst is generated by increased neuronal spiking activity in area 3b, recent non-invasive scalp recordings could not reveal concomitant single-trial added-activity, suggesting that the SEP burst might instead be generated by phase-reset of ongoing high-frequency EEG. Here, a statistical model and exemplary data are presented reconciling these seemingly contradictory results.
*Methods:* A statistical model defined the conditions required to detect added-activity in a set of single-trial SEP. Its predictions were tested by analyzing human single-trial scalp SEP recorded with custom-made low-noise amplifiers.
*Results:* The noise level in previous studies did not allow to detect single-trial added-activity in the period concomitant with the trial-averaged σ-burst. In contrast, optimized low-noise recordings do reveal added-activity in a set of single-trials.
*Conclusions:* The experimental noise level is the decisive factor determining the detectability of added-activity in single-trials. A low-noise experiment provided direct evidence that the SEP σ-burst is at least partly generated by added-activity matching earlier invasive single-cell recordings.
*Significance:* Quantitative criteria are provided for the feasibility of single-trial detectability of band-limited added-activity.


## 1. Introduction

Somatosensory evoked potentials (SEP) as well as magnetic fields evoked after median nerve stimulation contain high-frequency oscillations at around 600 Hz that are superimposed on the initial cortical component (N20; Cracco and Cracco, 1976; Curio et al., 1994; Hashimoto et al., 1996). This high-frequency oscillation consists of a brief burst of EEG/MEG activity, labeled here '$\sigma$-burst'. In the averaged wideband median nerve SEP it can be described as a few ripples riding on the N20 which can be isolated by high-pass filtering above 400 Hz.

While low-frequency EEG and MEG (<100 Hz) such as the N20 are generated mainly by postsynaptic mass activity (Okada et al.,

* Corresponding author. Address: Neurophysics Group, Department of Neurology, Campus Benjamin Franklin, Charite-University Medicine Berlin, Hindenburgdamm 30, 12203 Berlin, Germany. Tel.: +49 30 8445 2276; fax: +49 30 8445 4264.
*E-mail address:* gunnar.waterstraat@charite.de (G. Waterstraat).

1388-2457/$36.00 
http://dx.doi.org/10.1016/j.clinph.2012.03.013

1997) it was proposed that the concomitant high-frequency EEG (hfEEG) reflects spiking activity (Curio et al., 1994; Hashimoto et al., 1996; Curio, 2004). This hypothesis is supported by simultaneous macroscopic EEG and invasive single-cell measurements in non-human primates showing that the epidural macroscopic $\sigma$-burst is coincident with spike bursts of single neurons in the primary somatosensory cortex. Importantly, it was found that these bursting neurons have a low spontaneous activity and increased their activity in response to the peripheral stimulation (Baker et al., 2003). If hfEEG is indeed related to spiking activity one would predict that the observed increase of single-cell firing rates corresponds to added activity in the concomitant hfEEG. Yet, a recent study on human SEP recorded non-invasively at the scalp found no evidence for an amplitude increase of single-trial hfEEG during the $\sigma$-burst period; instead, an observed increase of inter-trial phase coherence (ITC) without significant changes in mean EEG activity lead to the conclusion that the SEP $\sigma$-burst might be generated by a phase-reset of ongoing high-frequency brain activity (Valencia et al., 2006). This interpretation is at variance with the prediction of added-activity based on invasive single-cell spike recordings. Could this difference be resolved eventually?

We suggest here that an analytical description of the experimental signal-to-noise ratio available in the respective experiments provides a framework that can accommodate all results available. As a starting point, we briefly review the three mechanisms presently discussed for the generation of an evoked component in trial-averaged recordings, i.e., added-activity, phase-reset, and transient baseline-shifts. In the added-activity model a stimulus-evoked component with constant amplitude and latency is added to the ongoing background EEG in each single-trial, which can then be isolated by averaging across trials. Phase-reset is defined as a stimulus-triggered transient alignment of background EEG oscillations in a given frequency band. As a result, peaks and troughs of the single-trial waveforms at that frequency do not cancel each other in the averaging process leading to a non-zero mean without net change of single-trial amplitude. Finally, transient baseline-shifts were proposed as a generator of slow evoked potentials (Nikulin et al., 2007) but they are more relevant for evoked responses in lower frequency bands.

A number of methods have been proposed to differentiate between phase-reset and added-activity (e.g. Sauseng et al., 2007). Notably, the presence of an evoked component in the averaged recording is per se an indicator of at least partial phase coherence across trials without differentiating between addition of a fixed-latency component or a phase-alignment of ongoing oscillations. Critically, as will be shown here, the detection of added single-trial activity, which would be the remaining criterion for advocating pro or con the added-activity model, is sensitive to noise contamination: For high noise levels there might be no chance to detect significant added-activity in single-trials—although potentially existent and possibly responsible for the generation of the evoked component in the average.

Scalp hfEEG includes technical noise and background brain activity which together can have an amplitude higher than the amplitude of stimulus-evoked components and thus impede the detection of added single-trial activity. This paper examines analytically the effect of noise on the detectability of changes in mean EEG power as compared to a baseline level. A model that allows to determine under what conditions an added component can be detected with statistical significance in a set of single-trials is used to resolve the seeming contradictions in previous studies on the mechanisms of evoked hfEEG generation. Finally, experimental evidence is presented supporting the predictions of that model.

## 2. Methods

### 2.1. Principle of statistical analysis for the detectability of single-trial added-activity

Based on the added-activity theory a model was derived to predict whether the detection of an added fixed-polarity, fixed-latency component in a limited set of single-trials is possible under a given signal-to-noise ratio. First, the minimal post-stimulus increase of single-trial EEG activity is predicted based on an averaged SEP under the assumption of the added-activity mechanism. Next, we compare this prediction to a noise estimate derived from baseline fluctuations in non-signal periods of the averaged waveform: If the evoked responses are generated by the added-activity mechanism, the single-trial SNR ($SNR_S$) can be derived directly from the ratio of rms amplitudes in signal and baseline windows in the averaged SEP (the root-mean square value, rms, of a signal is a measure of the mean amplitude of an amplitude-modulated signal). The complete derivation of this model and its assumptions can be found in Appendix A. Using the model equations one can then calculate the statistical power of a two-tailed $t$-test to detect the predicted post-stimulus increase of single-trial EEG activity. The statistical power is defined as the probability of rejecting the null hypothesis if it is indeed false, i.e., here the probability to detect a post-stimulus increase of single-trial EEG activity if it was actually present.

### 2.2. EEG recording

To demonstrate the critical influence of SNR on the single-trial detectability of changes in mean hfEEG amplitude, median nerve SEP were recorded in an optimized low-noise environment (shielded room; Vakuumschmelze AK3b) with custom-built amplifiers (Scheer et al., 2006). For all recordings, the stimulus consisted of electrical square-wave pulses of 200 μs duration with a constant-current intensity above motor threshold, eliciting a visible twitch of the thumb.

In a first step, single-channel recordings, presented in Scheer et al. (2011), were reanalyzed for this study. Median nerve SEP were recorded with three custom-built amplifiers providing different levels of intrinsic noise (white noise spectral density of $2.7\,nV/\sqrt{Hz}$, $4.8\,nV/\sqrt{Hz}$, or $12\,nV/\sqrt{Hz}$). The subject was a 49-year-old healthy male, known to exhibit a prominent $\sigma$-burst, whose right median nerve was stimulated at the wrist with a repetition rate of 5.21 Hz. About 6300 stimulation epochs were recorded within a bandwidth of 0.16–2000 Hz using a sampling frequency of 5 kHz at scalp position C3′ with a frontal reference at FC3. The stimulus artifact was removed by linear interpolation between −3 ms and 5 ms around the stimulus to avoid ringing of the digital filters applied off-line.

In a second step, multi-channel EEG data were acquired in four male subjects (26–49 years) using a 30-channel recording system with a white noise spectral density of $4.8\,nV/\sqrt{Hz}$ in the same shielded low-noise environment. To compare the results with the single-channel recordings the same subject was also included in the second experiment. The electrodes were distributed over both hemispheres preferentially over frontocentral and parietal regions to cover sensorimotor cortices (reference placed at nasion). Electrical stimulation was applied to the wrist with a per-side stimulation frequency of 5 Hz (in one subject to the right wrist, in three subjects alternating to the left and right wrist). The stimulus artifacts were removed by linear interpolation in a window from 3 ms before to 5 ms after the stimuli. For further analysis current source densities (CSDs, see below) were calculated, band-pass filtered and trial-averaged independently for right-hand and

left-hand stimuli. For single-trial analysis the channel with the highest amplitude ratio between a burst window and a late noise period in the trial-averaged band-pass filtered recordings (Rms Amplitude Ratio in the Average, RARA) was chosen.

A written informed consent was obtained from each subject. The experimental procedure was in accordance with decisions of the ethics committee of the Charite-University Medicine Berlin.

### 2.3. Current source density estimation

While in the first experiment a subject known to have a strong $\sigma$-burst response was chosen and median nerve SEP were recorded in a single bipolar derivation, in the second experiment median nerve SEP were recorded from three additional naive volunteers at multiple sites of the scalp with the reference placed at nasion (see above). In order to take advantage of the spatial spreading of EEG activity across the scalp, in these recordings a spatial filter was used. Specifically, current source densities (CSD) were estimated since they remove the effects of a common reference and provide a better localization of EEG components on the scalp (Perrin et al., 1987). Here we estimated CSDs using spherical splines (Perrin et al., 1989; corrigenda in Perrin et al., 1990) using well-established parameters (spline flexibility $m = 4$, $n = 50$ iterations, smoothing constant $\lambda = 10^{-5}$; Kayser and Tenke, 2006).

### 2.4. Time–frequency analysis

The amplitude of $\sigma$-bursts was localized in time–frequency maps calculated by means of the Stockwell transform (S transform; Stockwell et al., 1996), thus adopting the analysis approach of the previous study reporting the absence of added-activity in single-trials (Valencia et al., 2006). The S transform is a generalization of the short-term Fourier transform (STFT), offering frequency-dependent temporal resolution and thus optimizing the time localization in each frequency bin while maintaining the properties of the Fourier spectrum, such as absolute reference to phase.

The S transform amplitude map of the averaged SEP provides an estimate of the time–frequency resolved amplitude fluctuations that are at least partially phase-coherent across single-trials. Statistical testing was performed with a bootstrapping technique (McCubbin et al., 2008): For each amplitude value of the S transform map the probability density function (pdf) was estimated. New $N = 400$ sets of 6300 trials were created by resampling with replacement from the original set of 6300 trials. By averaging these newly created trial-ensembles 400 surrogate averages and their corresponding S transform amplitude maps were formed. Additionally, for each point of the S transform amplitude maps of these surrogate averages the variance was estimated in a nested bootstrap from the averages of further $N_1 = 50$ trial-ensembles, resampled with replacement from the corresponding previously resampled set of trials. Then the pdf at each post-stimulus time point of the S transform map was compared to a range of pre-stimulus points (−70 ms to −20 ms) in the same frequency bin (McCubbin et al., 2008). The pre-stimulus time point resulting in the largest $p$-value was then used as a baseline for further statistical testing. To correct for multiple comparisons the Benjamini–Hochberg-Procedure was applied (Benjamini and Hochberg, 1995). This procedure controls the 'False-Discovery-Rate' (FDR), the maximal ratio of false positives amongst all test results that were declared significant. The null-hypothesis (i.e., no added-amplitude at a particular time–frequency point) was rejected if the two-tailed FDR was below $\alpha = 0.05$ and at the same time the probability of false negatives was estimated to be below 10% (McCubbin et al., 2008).

Analogously, the S transform amplitude map was calculated for each single-trial, and a logarithmic transform was applied to approximate normality replacing the heavily right-skewed untransformed amplitude distributions. The average of these single-trial transforms is an estimate of the time–frequency-resolved amplitude fluctuations that occur at a constant latency after the stimulus but do not have the requirement of inter-trial phase coherence. For statistical testing the variances were estimated from the set of S transforms of each single-trial. Each point in a column (the transformed amplitude spectrum at a post-stimulus time-slice) of the S transform was tested against that value in the pre-stimulus time-window (−70 ms to −20 ms) in the same frequency bin that yielded the highest $p$-value using Welch's $t$-test. A time–frequency point of the map was then considered significant if the two-tailed FDR was below $\alpha = 0.05$.

For the visualization of the S transform amplitude maps, the values were re-transformed to a linear scale and normalized by dividing each amplitude value by the median amplitude of the pre-stimulus noise window in that frequency bin.

In order to visualize comparable S transform amplitude maps of signal-free data as a control for the absence of spurious activations possibly introduced by the analysis pipeline, the same procedure was conducted on trials which were sampled from the ongoing wideband and band-pass filtered EEG channels without any temporal relation to the median nerve stimulation.

### 2.5. Time-resolved analysis of hfEEG responses

The $\sigma$-burst was isolated by band-pass filtering the broadband EEG (400–900 Hz digital zero phase delay FIR-filter, transition width 30 Hz, roll-off 0.16 dB/Hz). Trials for which the log-transformed rms amplitude exceeded the mean plus two standard deviations in a window covering the full response except the last 10 ms prior to the next stimulus were excluded from further analysis. In the trial-averaged hfSEP the ratio of rms values between the burst window (15–29 ms) and the baseline rms-value was determined (RARA). This baseline level in the trial-averaged response was calculated as the median of rms values calculated from a moving window of 14 ms length, moving along the averaged SEP from −70 ms to −20 ms pre-stimulus.

The time course of the rms amplitude in the band-pass filtered single-trials was estimated with a four-step procedure (Fig. 1). The distribution of rms values was determined in consecutive overlapping time-windows of 14 ms length each, shifted by 1 datapoint (0.2 ms) against each other. To correct for the right-skewed distribution of rms values a logarithmic transform was applied. Quantile–quantile plots showed a near-perfect agreement to a normal distribution after these pre-processing steps. Furthermore, the log-transformed rms values did not exhibit a noticeable trend across trials (the slope of a regression line was below 0.002% of the mean log-rms for all measurements). For each position of the 'sliding window' the mean and variance of the distribution of log-transformed rms values was determined. The median of these mean rms values and the pooled variance from all values in a window from −70 ms to −20 ms pre-stimulus were used as mean and variance of the baseline noise distribution. Student's two-sided $t$-test for independent samples was used to assess if the baseline and the distribution of log-transformed rms values for each post-stimulus location of the 'sliding window' could potentially have the same mean value (two-tailed $p < 0.05$). The corresponding confidence intervals were calculated for a 95% significance level. The observed difference of log-transformed rms values ($\Delta RMS_{\log}$) and the significance intervals were back-transformed to a linear scale and normalized as a percentage value above the baseline level ($\Delta RMS_{norm} = 100(e^{\Delta RMS_{\log}} - 1)$). The result of this procedure is the temporally-resolved normalized estimate of the modulation of single-trial high-frequency rms values, including significance intervals.

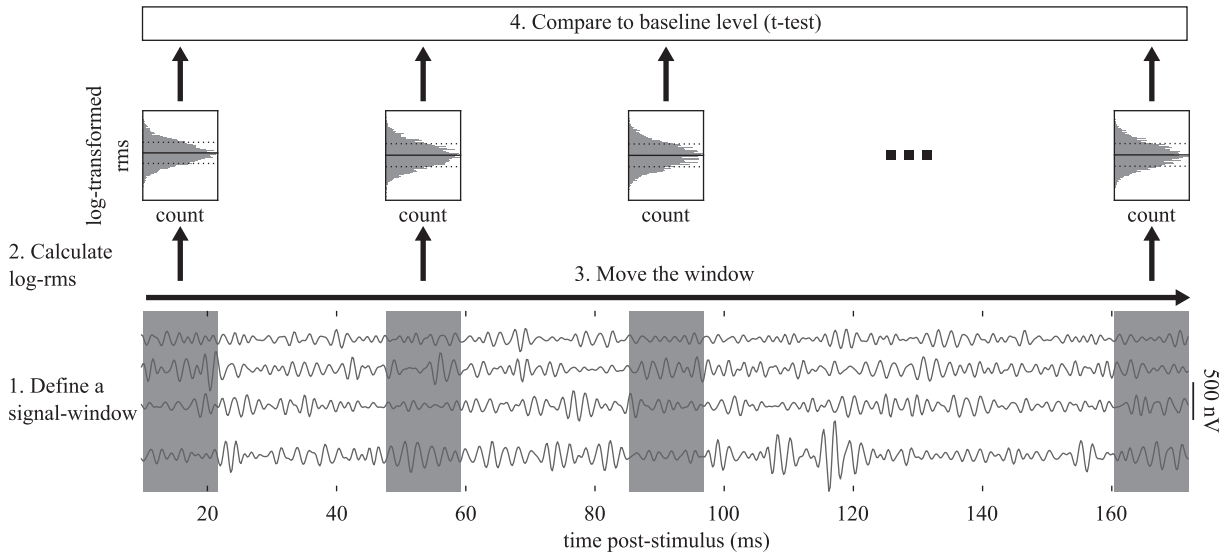


**Fig. 1.** The time course of rms values in single-trials was calculated with a four-step procedure: (1) A window with a length matched to the duration of the $\sigma$-burst was defined. (2) The logarithm of the rms value was calculated for each trial, resulting in a distribution of log-transformed rms values across trials for this period. (3) This window was slided progressively in time in steps of 0.2 ms and in each of the overlapping windows the mean and variance of those log-rms values was calculated. (4) Student's $t$-test was used to test whether each of the distributions in the 'sliding window' could possibly have the same mean as the baseline level (compare Section 2). Confidence intervals were estimated for a significance level of 95%.

To compare the amplitudes of the band-pass filtered single-trials and the averaged hfSEP, the amplitude-envelopes of the corresponding waveforms were computed as the magnitude of their discrete Hilbert transforms.

## 3. Results

### 3.1. Detectability of added-activity in single-trials

To reconcile the seemingly incompatible results of previous invasive single-cell spike recordings (Baker et al., 2003) and non-invasive EEG recordings (Valencia et al., 2006) the present study ascertains whether – given a particular experimental noise level – it is possible at all to detect added single-trial components in scalp EEG recordings. Their detectability depends, e.g., on SNR, trial-to-trial variability of the recorded EEG signal, and number of recorded trials. A statistical model including these parameters was developed, allowing to test under what experimental conditions one could be able to detect added signal activity in single-trials (see Section 2 and Appendix A).

This model requires the single-trial SNR ($SNR_s$) to be known. $SNR_s$ can be estimated from the ratio of rms signal and noise amplitudes in the average (RARA) under the assumption that the response was generated by means of the added-activity mechanism. As a second step, the power of a two-sample $t$-test to discriminate between the noise and signal window can be determined based on the previously estimated single-trial SNR (probability of type I error $\alpha = 0.05$).

From the data published in Valencia et al. (2006; Fig. 1, Channel C3) RARA was estimated to be approximately RARA = 4. Given the number of trials the authors acquired ($N \approx 2000$) the single-trial signal-to-noise ratio can be estimated as $SNR_s = 0.087$ under the model assumptions given in Appendix A. Assuming a signal length of 18 data points (15 ms sampled with a sampling-frequency of 1.2 kHz—twice the bandwidth of the applied band-pass filter), it can be concluded that the SNR available in that study did not provide a fair chance to find significant added components in single-trials (power of a two-sided $t$-test with $\alpha = 0.05$: $1 - \beta = 0.11$). Actually, the statistical model predicts that with this experimental setup at least 41823 trials would be required to achieve a test power of $1 - \beta = 0.9$. Therefore, the experimental conditions did not provide a possibility to conclude about true mechanisms of $\sigma$-burst generation.

### 3.2. Single-trial detection of added high-frequency components in human SEP

In order to be able to detect added-activity in single-trials it is necessary to use either an excessive number of independent trials, or to increase the effective signal-to-noise ratio. To this end, EEG data was acquired in a shielded recording chamber using custom-engineered low-noise EEG amplifiers (see Section 2). Moreover, in a piloting experiment (Scheer et al., 2011) a subject with a prominent $\sigma$-burst visible in the averaged SEP was chosen and a large number of trials ($n = 6329$) was collected.

The subject exposed a clear N20 with visually detectable 'ripples' riding on it. When applying a Stockwell transform to the averaged wideband SEP the resulting normalized amplitude maps (see Section 2) showed a significant activation at around 20 ms (Fig. 2, left side) in the high-frequency range ($f > 400$ Hz, $p < 0.05$), coinciding with a low-frequency activation (0–400 Hz).

For a quantitative analysis of single-trial energy fluctuations in the high-frequency range the limits of the band-pass filter were chosen to span the range from 400 Hz to 900 Hz. Averaging the band-pass filtered single-trials isolated the $\sigma$-burst. For the amplifier with a white noise level of $2.7\,\mathrm{nV}/\sqrt{\mathrm{Hz}}$ the ratio of rms values of the $\sigma$-burst and baseline rms in the average was RARA = 24.5 (number of trials $n = 6300$), for the amplifier with a noise level of $4.8(12)\,\mathrm{nV}/\sqrt{\mathrm{Hz}}$ this value was only 23.2 (24.1). Based on these values (Table 1) and the statistical model (cf. Appendix A) it should be possible to detect a potential added component in the set of recorded single-trials (power of a two-sided $t$-test $(1 - \beta) \approx 1$, two-sided significance level $\alpha = 0.05$).

Exploiting this result, the time–frequency analysis was applied on the single-trial data to probe the presence of added high-frequency activity in single-trials. Again, a significant amplitude increase in the high-frequency range (Fig. 2, right side) was detected congruent with the activation described in the average response.

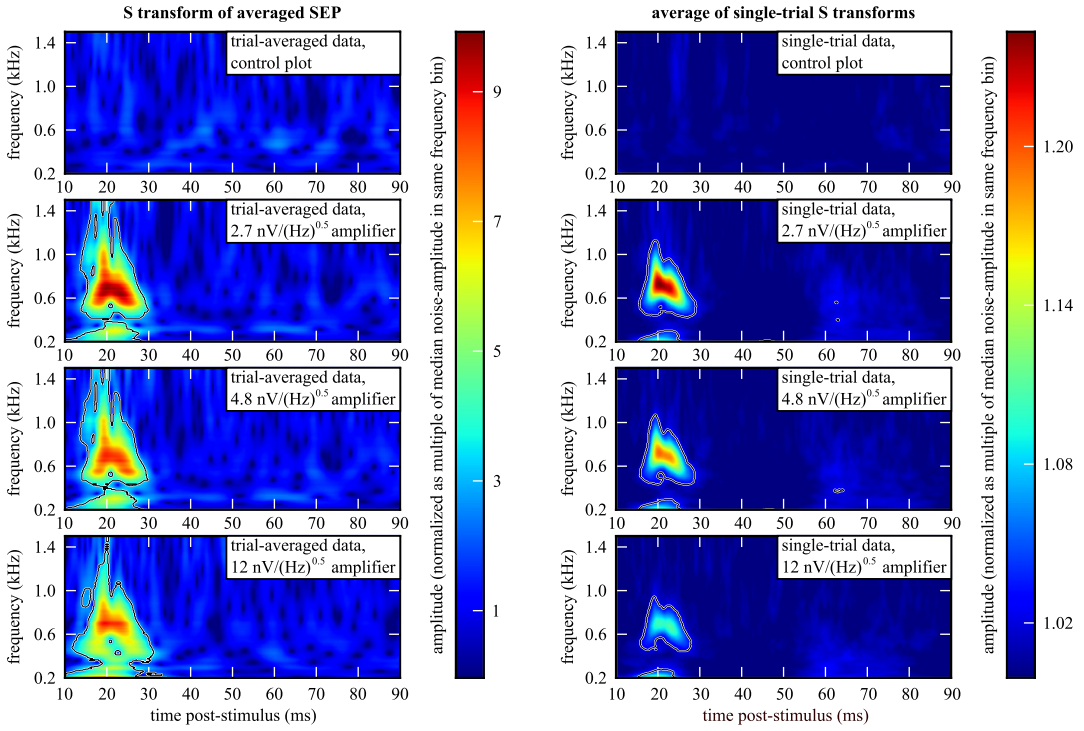


**Fig. 2.** S transform amplitude spectra. Black contours enclose areas that were declared significant after correction for multiple-comparisons using the Benjamini–Hochberg procedure with $\alpha = 0.05$ (and $(1 - b) > 0.9$ for S transforms of averaged SEP). Amplitude values were normalized by dividing them with the median of the amplitudes in a window from −70 to −20 ms pre-stimulus in that frequency bin for adequate visualization. Left: S transform amplitude spectra of average. Right: Averaged S transform of amplitude spectra of single-trials. Top: Control maps were generated from trials which were sampled from the original data without temporal relation to the median nerve stimulation. Second (3rd, bottom panel): Amplifier with noise level of $2.7\,nV/\sqrt{Hz}$ ($4.8\,nV/\sqrt{Hz}$, $12\,nV/\sqrt{Hz}$). In all maps there is a clear activation at around 20 ms in the 400–1150 Hz range. In the single-trial transforms the amount of this activation is largest for the amplifier with the lowest noise level and drops continuously for the amplifiers with higher noise levels. For the transform of the averaged SEP the single-trial noise amplitude is less important for the detection of this activation. The shape of the activations in the single-trials is similar to the corresponding activation in the average.

This activation was well localized in the time–frequency plane, centered around 20 ms in a frequency band of about 425–1115 Hz. Moreover, the sigma-burst component was well separated from low-frequency activations.

Notably, the time–frequency significance limits of the single-trial $\sigma$-burst differ from the limits reported for the averaged SEP. Presumably, these differences are due to the higher noise contributions in the single-trial data which mask the low-amplitude components and decrease their detectability. This presumption is supported by the finding that the frequency limits of the significant activations differed depending on the noise level of the used amplifier. Signals recorded with the best amplifier exposed the highest increase of EEG amplitude during the burst period as compared to the median amplitude in a noise baseline window (−70 ms to −20 ms) and, at the same time, the broadest significance limits ($2.7\,nV/\sqrt{Hz}$ amplifier: 425–1115 Hz) compared to the amplifiers with less favorable noise levels ($4.8\,nV/\sqrt{Hz}$ amplifier: 425–1050 Hz, $12\,nV/\sqrt{Hz}$ amplifier: 450–950 Hz).

To assess quantitatively the amplitude fluctuations in the band-pass filtered single-trials a simple yet effective approach was used that works in the time domain (Fig. 1): in a four-step procedure log-transformed rms amplitudes in post-stimulus time-windows were compared to a baseline amplitude estimate using Student's t-test for independent samples. This test procedure showed a peak of added-activity in the band-pass filtered single-trials at about 20 ms (Fig. 3). Similar to the result of the S transform analysis the amount of detectable added rms amplitude was clearly dependent on the band-limited amplifier noise: The higher the noise level of the amplifier the lower the detectable amount of added rms amplitude (*cf.* Table 1). Fig. 3 also shows some amplitude

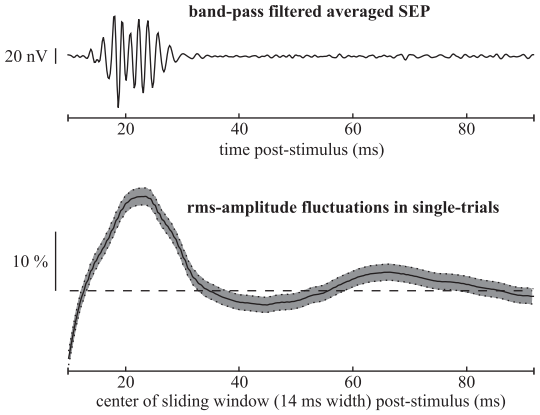


**Fig. 3.** Averaged high-frequency SEP and rms amplitude fluctuations in band-pass filtered single-trials for the single-channel recording of the first subject with the amplifier providing a noise level of $2.7\,nV/\sqrt{Hz}$. Top: Average of band-pass filtered single-trials. Bottom: rms amplitude in a sliding window as relative deviation from the baseline level. Gray-shaded area indicates the 95% confidence intervals of Student's *t*-test. There is a highly significant increase of rms amplitudes at around 20 ms, precisely coinciding with the $\sigma$-burst in the average. Additional peaks did not have an equivalent in the average, indicating insufficient phase and latency synchronization. Similar results, although with a smaller amplitude were found for the other amplifiers.

fluctuations coinciding with late near-threshold activations in the single-trial S transform amplitude maps (55–75 ms); their characteristics are subject of follow-up studies.

To corroborate these pilot findings, median nerve SEP were recorded in additional three subjects (in two of them with

**Table 1**
Summary of results.

| Measurement | | | | | | Statistical detectability analysis | | | | Result |
|---|---|---|---|---|---|---|---|---|---|---|
| S | H | Ref. | Amp. noise (nV/Hz$^{½}$) | *N* | Burst rms (nV\|nV/cm$^2$) | RARA | $SNR_s$ | $\sigma_{RMSlog}$ | Test-power(%) | $\Delta RMS_{norm}$(%) |
| Experiment 1 | | | | | | | | | | |
| 1 | L | Bipolar | 2.7 | 6326 | 79.92 | 24.5 | 0.31 | 0.43 | 100 | **17.60** |
| | | | 4.8 | | 80.04 | 23.2 | 0.29 | 0.4 | 100 | **14.50** |
| | | | 12.0 | | 79.51 | 24.1 | 0.3 | 0.3 | 100 | **8.90** |
| Experiment 2 | | | | | | | | | | |
| 1 | L | CSD | 4.8 | 15,470 | 5.27 | 43.9 | 0.35 | 0.31 | 100 | **11.60** |
| | R | | | | 4.71 | 21.5 | 0.17 | 0.31 | 98.6 | **8.40** |
| 2 | L | CSD | 4.8 | 15,469 | 2.61 | 22.2 | 0.18 | 0.25 | 100 | **2.20** |
| | R | | | | 3.77 | 26.4 | 0.21 | 0.28 | 100 | **2.00** |
| 3 | L | CSD | 4.8 | 10,817 | 0.5 | 5.1 | 0.05 | 0.3 | 4.7 | 0.30 |
| | R | | | | 0.98 | 10.4 | 0.1 | 0.31 | 21.7 | 0.80 |
| 4 | L | CSD | 4.8 | 11,977 | 0.55 | 4.9 | 0.04 | 0.36 | 4 | 0.60 |

S: subject number, H: hemisphere (L: left hemisphere, R: right hemisphere), Ref.: reference electrode, bipolar or current source densities (CSDs), Amp. noise: noise spectral density of the used EEG amplifier. N: number of recorded trials, Burst rms: rms–amplitude in a window of 14–29 ms in the band-pass filtered average. RARA: Rms Amplitude Ratio in the Average, SNR of the trial-averaged SEP. $SNR_s$: estimated single-trial SNR, as estimated by formula (10). $\sigma_{RMS_{log}}$: pooled standard deviation of log-transformed rms values in the baseline window. Test-power: estimated statistical power to detect an increase of activity in single-trials. Estimated by Eq. (19). $\Delta RMS_{norm}$: Difference between burst rms and baseline rms, normalized to the baseline level in percent. Significant values are marked in bold print. The burst amplitudes of the four subjects spanned a broad range from strong to weak responses. The statistical detectability analysis proved instrumental in identifying recordings for which the detection was possible. For those recordings exhibiting a strong average burst response, large values for the statistical power were estimated. These values were generally low in recordings for which no increase of single-trial activity could be demonstrated.

alternating bilateral stimulation) with a 30-channel system. In order to improve the signal-to-noise ratio in the second experiment a spatial filter was applied to the multiple-channel data. Current source densities (CSDs) were chosen for the analysis because they remove the effects of common reference and provide a better spatial localization of the EEG on the scalp (Perrin et al., 1987). Individually, the channel with the most prominent burst response in the average (largest RARA) was chosen for further analysis. The subject of the first experiment was included again (Table 1, subject 1) to test for the reproducibility of the previously described results. Confirming the results of the first experiment this subject exposed a $\sigma$-burst that could be demonstrated in the average SEP and as added-activity in single-trials. Moreover, the analysis was repeated also for his previously untested right hemisphere, yielding positive results also in that hemisphere.

For the additional subjects of the second experiment the added amplitude during the burst window was identified with statistical significance in two of five CSD data (exemplary single-trial S transform amplitude maps for subjects 2–4 are presented in Fig. 4). For the cases in which no significant added-activity was detected a statistical power below 22% was estimated whereas for the positive cases it was larger than 98%. These results could mainly be attributed to the individual $\sigma$-burst amplitude in the averaged high-frequency CSD. While for the first and second subjects high and intermediate $\sigma$-burst rms-amplitudes (2.6–5.3 nV/cm$^2$) in the CSD-averages were recorded, subjects three and four exhibited considerably lower $\sigma$-burst rms-amplitudes (0.5–1.0 nV/cm$^2$, Table 1). In agreement with the conducted statistical detectability analysis no significant added evoked activity was detected for those subjects.

In all but one cases (subject 2, right hemisphere $\sigma$-burst) the measured increase of single-trial amplitude in the $\sigma$-burst time-window ($\Delta RMS_{norm}$) was higher than predicted by the statistical detectability analysis. In absolute values, $\Delta RMS_{norm}$ was on average 3.16% larger than expected (two-tailed $p = 0.01$, 95% confidence interval 0.18–5.89%, Wilcoxon signed rank test). The ratio between the measured and predicted $\Delta RMS_{norm}$ was on average 2.13 (95% confidence interval 1.4–2.9) indicating that a large fraction of the single-trial added-activity suffered from latency-jitter or that additional non-phase-locked added-activity in single-trials was present (i.e., induced activity).

In summary, we tested for a significant increase in single-trial activity in four subjects spanning the natural range of high (subject 1), intermediate (subject 2) and low (subjects 3 and 4) $\sigma$-burst strengths. While for strong and intermediate $\sigma$-bursts added single-trial activity could constantly be demonstrated after application of a simple spatial filter, this was not possible for subjects characterized by low $\sigma$-burst amplitudes (cf. Fig. 4). This is in agreement with the presented detectability analysis.

To further illustrate the different detectability of added-activity in cases of different SNR, the mean power-envelope of band-pass filtered single-trials and of the averaged hfSEP were compared for subjects with either strong or weak $\sigma$-burst responses: For subject 1 there is a clear increase of the power-envelope in the averaged hfSEP (Fig. 5: black solid line) as well as in the band-pass

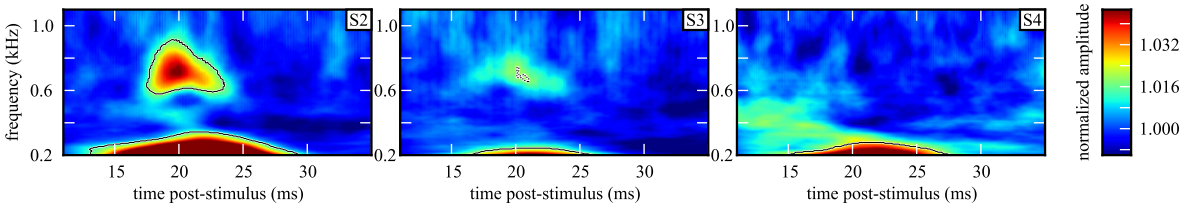


**Fig. 4.** Single-trial S transform amplitude maps for subjects S2, S3 and S4. Black solid contours enclose areas of significant amplitude change (two-tailed FDR $\alpha \leqslant 0.05$ after correction for multiple-comparisons using the Benjamini–Hochberg procedure). While in subject 2 (right-hemisphere response shown) there is a significant amount of added-activity during the signal window in the frequency band of the $\sigma$-burst, this is not the case for subjects 3 (right-hemisphere response shown) and 4 (left-hemisphere response shown). This is attributable to low $\sigma$-burst amplitudes in the averaged hfSEP (cf. Table 1; note change in color scale in comparison to Fig. 2, right panel). Notably, subject 3 is an interesting borderline case with an apparent added-activity at 20 ms and about 700 Hz in the single-trial S transform amplitude map (as for S1 and S2) which, however, missed significance (two-tailed FDR $\alpha = 0.3$; dotted line). Using this FDR for the other subjects did not result in a noteworthy change of the shown significance borders.

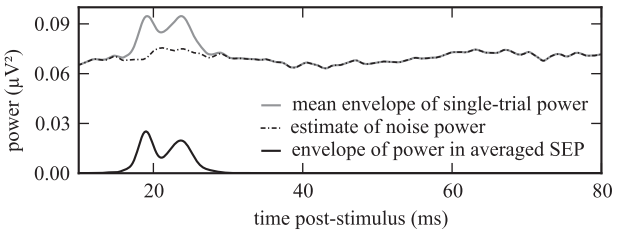


**Fig. 5.** Average power-envelope of band-pass filtered single-trials (gray solid line) and power-envelope of the averaged hfSEP (black solid line; subject 1, experiment 1). Under the assumptions of the added-activity theory subtraction of the averaged hfSEP from the single-trials results in noise (black dash-dotted line). During the $\sigma$-burst time-window (~20 ms) there is a clear increase of the mean single-trial power in subject 1 in whom the ratio between the power-envelope of the averaged hfSEP and the mean power-envelope in single-trials during the $\sigma$-burst time-window is large ($\approx 0.25$).

filtered single-trials (gray solid line) during the $\sigma$-burst time-window. Under the assumptions of the added-activity model, i.e., for an infinite number of recorded trials the averaged hfSEP approaches a noise-free estimate of the added-activity, the added-activity can be removed from the single-trials by subtracting the power of the hfSEP from the power in single-trials. Clearly, for subject 1 the mean power-envelope of measured single-trials (gray solid line) in the $\sigma$-burst time-window is larger than in case of "signal-depleted" trials (black dash-dotted line) by about 25%. Contrary, for subject 4 this difference between measured and "signal-depleted" single-trial power (i.e., noise) is as low as 1% (data not shown) and, consequently, cannot be discriminated. This corresponds to a low single-trial SNR.

## 4. Discussion

Brains process information continuously and adapt to a changing environment. Therefore, when examining the relation between processing of external stimuli, pre-stimulus brain states, variable behavioral reactions, and concomitant electromagnetic brain activity, a single-trial analysis would be advantageous. Often, however, SNR impedes single-trial EEG analyses: For low SNR, the single-trials might be dominated by noise to such extent that added-activity could be missed easily. Therefore, the absence of evidence for added-activity does not inevitably imply evidence for its absence. The power of statistical testing to detect a potential amplitude increase will be low if the amount of added-activity present in single-trials is small in relation to the noise level, i.e., statistical tests are prone to yield false negative results.

The goal of the present study was to assess the probability of detecting evoked 600 Hz activity within a set of single-trials including ongoing background EEG. To this end, we developed a statistical model that quantifies the statistical power of detecting an additive component in a set of single-trial evoked responses and that allows to estimate the number of stimulation epochs required to reach a desired statistical power for a given combination of signal strength and band-limited noise. This model is general and can be applied to compare contributions from time and phase-locked components and examine their impact on the average response.

Here, we studied possible generator mechanisms of evoked 600 Hz SEP components ($\sigma$-bursts). A recent study reported the absence of an amplitude increase in single-trials during the $\sigma$-burst time-window and concluded that $\sigma$-bursts are generated by a phase-reset of ongoing EEG oscillations rather than by added-activity (Valencia et al., 2006). In line with previous arguments (Jansen et al., 2003; Rizzuto et al., 2003; Shah et al., 2004), the authors regarded post-stimulus phase concentration and the absence of added-activity in single-trials as evidence for a main contribution of phase-reset to the generation of hfSEP. Meeting these criteria, however, is not sufficient to exclude the generation of evoked potentials by additive components (Sauseng et al., 2007). Actually, the present results reveal that owing to experimental noise a study might not have a fair chance to detect such additive components on the single-trial level with a reasonable number of recorded stimulation epochs; e.g., in Valencia et al. (2006) the number of trials required to reach a statistical power of 0.9 was estimated as $N > 41823$.

The optimized experimental setup that was established in Scheer et al. (2011) minimized technical noise contributions, thus permitting the detection of added single-trial activity with a relatively small number of trials (the number of trials to achieve a statistical power of 0.9 was estimated as $N > 226$). The single-trial analysis of this low-noise recording clearly uncovered an increase of single-trial hfEEG amplitude during the $\sigma$-burst time-window. This result was confirmed in both hemispheres of two subjects with high and intermediate $\sigma$-burst amplitudes in the averaged hfSEP, providing exemplary evidence for the contribution of an additive mechanism to the $\sigma$-burst generation. In agreement with the presented detectability analysis, added-activity in single-trials could not be uncovered in subjects with a low $\sigma$-burst amplitude.

Notably, the measured increase of single-trial activity in the $\sigma$-burst window was on average 2.13 times larger than the increase predicted by the statistical detectability analysis. This could indicate that latency-jitter greatly diminishes the effect of this activity on the averaged SEP or that additional 'induced' activity occurs during the $\sigma$-burst window. The investigation of both possibilities remains subject of follow-up studies.

It has been recently argued that the detection of added-activity in single-trials of EEG does not determine the mechanisms of evoked response generation at the microscopic neuronal level (Telenczuk et al., 2010). However, in accordance with the conclusion of the present non-invasive study, invasive measures in the barrel cortex of rats (Barth, 2003) and the primary somatosensory cortex of non-human primates (Baker et al., 2003) have shown that macroscopic evoked hfSEP are related to increased activity at both, single-cell and population level. Characteristically, the intracranial recordings used in these studies allowed to obtain an excellent signal-to-noise ratio, and thus enabled the detection of significant increase of spike-rate and electric field potentials in single-trials.

The identification of the $\sigma$-burst on the single-trial level using a dedicated low-noise scalp EEG set-up as described here opens the possibility to study the physiological variability of $\sigma$-burst latency, phase and amplitude non-invasively. Amplitude and latency modifications of the $\sigma$-burst in the averaged hfSEP have been observed under a variety of conditions, such as reduced attention (Gobbelé et al., 2000), NREM sleep (Yamada et al., 1988; Hashimoto et al., 1996; Hashimoto, 2000), general anesthesia or sedation (Haueisen et al., 2000; Klostermann et al., 2000b; Urasaki et al., 2006), age (Nakano and Hashimoto, 2000), certain diseases (Mochizuki et al., 1999; Alegre et al., 2006), and different stimulation paradigms (Klostermann et al., 1998; Klostermann et al., 1999; Klostermann et al., 2000a). The single-trial analysis of hfEEG may therefore provide a new means to study and understand the interplay between pre-stimulus state of the brain and extrinsic influences on evoked activity.

Altogether these findings fuel the expectation that the $\sigma$-burst offers a possibility to examine the electrical activity of spiking cortical neurons with macroscopic scalp EEG.

## Acknowledgements

G.W., B.T. and G.C. acknowledge support from SFB 618 (Project B4). G.C., M.B., T.F. and H.J.S. acknowledge support from Bernstein Focus Neurotechnology (Project B1).

## Appendix A. Statistical SEP detectability analysis

An analytical model of the added-activity theory was derived which aimed at answering the following questions: (1). For a specific signal-to-noise ratio observed in the average (Rms-Amplitude Ratio in the Average, RARA) what was the band-limited noise in the single-trials during the response period that would explain this RARA? (2). Given this noise and the number of trials is it possible to detect the signal as added-activity with statistical significance?

In the added-activity theory the measured EEG signal in each trial k is the compound $c_k(t)$ of a noise part $n_k(t)$ and an added signal part $s(t)$, which is constant in all trials with the total number of trials $N$.

$$c_k(t) = s(t) + n_k(t) \text{ for } k = 0, 1, \ldots N-1. \tag{1}$$

The root mean square value (rms value) of a signal in a predefined time-window is a measure of the signal's mean amplitude during that period. The rms value of a signal $x(t)$ in a time-window from 0 to T is given by:

$$RMS(x(t)|_{t=0}^{T}) = \sqrt{\frac{\sum_{t=0}^{T} x(t)^2}{T}}. \tag{2}$$

Similarly, one can calculate the expected rms value of the noise by averaging the single-trial rms across all trials:

$$\langle RMS(n(t))\rangle = \frac{1}{N}\sum_{k=0}^{N-1} RMS(n_k(t)|_{t=t_0}^{t_0+T}) \tag{3}$$

where $\langle\cdot\rangle$ denotes the average across trials.

The estimate of SNR in a single-trial is defined here as the quotient of the rms value of the signal $RMS(s(t))$ and the mean rms value of the noise, calculated across all trials:

$$SNR_S = \frac{RMS(s(t))}{\langle RMS(n(t))\rangle}. \tag{4}$$

Since the rms value of the isolated signal is usually unknown this measure cannot be routinely used in practice. Instead, rms amplitudes of a 'signal window' and a 'noise window' in the average can be compared. Naturally, this signal window still contains some noise contribution, the amount of which, however, greatly diminishes with the total number of trials.

The ratio of rms amplitudes calculated within signal ($t_1 < t < t_1 + T$) and noise ($t_0 < t < t_0 + T$) windows in the average (RARA) is defined as:

$$RARA(N) = \frac{RMS(\langle c_k(t)|_{t=t_1}^{t_1+T}\rangle)}{RMS(\langle c_k(t)|_{t=t_0}^{t_0+T}\rangle)}, \quad \text{with} \quad t_0 + T < 0 \quad \text{and} \quad t_1 > 0 \tag{5}$$

Since in the noise window ($t_0 < t < t_0 + T < 0$) the signal component $s(t) = 0$, RARA can equivalently be expressed as:

$$RARA(N) = \frac{RMS\left(s(t)|_{t=t_1}^{t_1+T} + \langle n_k(t)|_{t=t_1}^{t_1+T}\rangle\right)}{RMS\left(\langle n_k(t)|_{t=t_0}^{t_0+T}\rangle\right)}, \text{ with } t_0+T<0 \text{ and } t_1>0 \tag{6}$$

The restriction $t_0 + T < 0$ is used to define a pre-stimulus period for the noise window.

As the noise is not locked to the stimulus, in the averaged response it will be increasingly diminished with a higher number of trials. Hence, the definition of RARA yields a higher value for a greater number of trials. In the limit of $N \to \infty$ it tends to infinity.

For practical reasons it will be assumed that the noise contribution in the average is equal during both time-windows. This assumption is correct insofar as each stimulus-locked component can be defined to be a part of $s(t)$.

Determinants of the RARA in this model are: the SNR in the single-trials ($SNR_S$) and the number of trials N. Both have an algebraic relation under the following assumptions: (i) the averaged SEP is generated by an added component, (ii) noise and signal are uncorrelated, (iii) noise in different trials is independent and identically distributed, (iv) the signal is identical in all trials in terms of amplitude, latency and phase, and (v) there is no signal during the noise window. Then the following relationships hold true:

$$\begin{aligned} RMS\left(\langle c_k(t)|_{t=t_1}^{t_1+T}\rangle\right) &= \sqrt{RMS\left(s(t)|_{t=t_1}^{t_1+T}\right)^2 + \frac{\left\langle RMS\left(n_k(t)|_{t=t_1}^{t_1+T}\right)\right\rangle^2}{N}} \\ &\approx \left((SNR_S \cdot \left\langle RMS\left(n_k(t)|_{t=t_1}^{t_1+T}\right)\right\rangle)^2 \right. \\ &\quad \left. + \left\langle RMS\left(n_k(t)|_{t=t_1}^{t_1+T}\right)\right\rangle^2/N\right)^{\frac{1}{2}} \\ &\approx \left(\sqrt{SNR_S^2 + \frac{1}{N}}\right) \cdot \left\langle RMS\left(n_k(t)|_{t=t_1}^{t_1+T}\right)\right\rangle \\ &\approx \left(\sqrt{SNR_S^2 + \frac{1}{N}}\right) \cdot \left\langle RMS\left(n_k(t)|_{t=t_0}^{t_0+T}\right)\right\rangle \end{aligned} \tag{7}$$

and

$$RMS\left(\left\langle n_k(t)|_{t=t_0}^{t_0+T}\right\rangle\right) = \frac{\left\langle RMS\left(n_k(t)|_{t=t_0}^{t_0+T}\right)\right\rangle}{\sqrt{N}}. \tag{8}$$

Then $RARA(N)$ equals:

$$\begin{aligned} RARA(N) &= \frac{RMS\left(\left\langle c_k(t)|_{t=t_1}^{t_1+T}\right\rangle\right)}{RMS\left(\left\langle n_k(t)|_{t=t_0}^{t_0+T}\right\rangle\right)} \\ &\approx \frac{\left(\sqrt{SNR_S^2 + \frac{1}{N}}\right) \cdot \left\langle RMS\left(n_k(t)|_{t=t_0}^{t_0+T}\right)\right\rangle}{\left\langle RMS\left(n_k(t)|_{t=t_0}^{t_0+T}\right)\right\rangle/\sqrt{N}} \\ &\approx \sqrt{SNR_S^2 \cdot N + 1} \end{aligned} \tag{9}$$

which can be rearranged to:

$$SNR_S \approx \sqrt{\frac{RARA(N)^2 - 1}{N}} \tag{10}$$

The comparison of the mean single-trial amplitudes between the signal and the noise window can be expressed as the difference between the mean rms values in these windows ($\Delta RMS$):

$$\Delta RMS = \left\langle RMS\left(c(t)|_{t=t_1}^{t_1+T}\right)\right\rangle - \left\langle RMS\left(n(t)|_{t=t_0}^{t_0+T}\right)\right\rangle. \tag{11}$$

Empirically, the distribution of the single-trial rms values approximated a log-normal distribution. The following relationship exists for $\Delta RMS_{\log}$, the difference of the log-transformed single-trial rms values, under the above assumptions:

$$\begin{aligned} \Delta RMS_{\log} &= \left\langle \log\left(RMS\left(c_k(t)|_{t=t_1}^{t_1+T}\right)\right)\right\rangle \\ &\quad - \left\langle \log\left(RMS\left(n_k(t)|_{t=t_0}^{t_0+T}\right)\right)\right\rangle \\ &\approx \log\sqrt{\left(SNR_S^2 + 1\right) \cdot \left\langle RMS\left(n_k(t)|_{t=t_0}^{t_0+T}\right)\right\rangle^2} \\ &\quad - \log\left(\left\langle RMS\left(n_k(t)|_{t=t_0}^{t_0+T}\right)\right\rangle\right) \\ &\approx 0.5\log(SNR_S^2 + 1). \end{aligned} \tag{12}$$

It should be noted, that due to the simplification in Eq. (12) it must be assumed that the distribution of rms values in the signal and the

noise window are similar to each other, such that the log transform has a similar effect on both, and that the relative difference of their means remains unchanged.

In practice other transformations such as box-cox power transformations might be valuable tools for normalizing the data. For the high number of trials that is usually used in SEP acquisition the t-test is fairly robust against non-normality (Sachs and Hedderich, 2006), and such a log transform offers sufficiently strong power.

With the formulas introduced one can predict the single-trial SNR from the amplitude ratio in the average. The detectability of the difference between the signal and the noise window in real-data EEG experiments is dependent on $SNR_S$ and the variability of the single-trial rms values. A high variability will easily mask any amplitude fluctuation in single-trials and prevent its detection.

In this derivation Student's t-test was used to calculate whether this difference could be detected with significance. The null hypothesis of $\Delta RMS_{\log} = 0$, meaning that the mean rms values in the noise and signal window are equal (i.e., no added-activity), can be rejected if:

$$t \leqslant \frac{\Delta RMS_{\log}}{\sigma_{RMS_{\log}}} \sqrt{\frac{N}{2}}, \tag{13}$$

where $\sigma_{RMS_{\log}}$ is the standard deviation of the log-transformed rms values. It is assumed to be equal in the signal and noise window. Using the log-transform in the definition of $\sigma_{RMS_{\log}}$ has the advantage that $\sigma_{RMS_{\log}}$ is hereby directly related to the coefficient of variation of the untransformed rms values and as such a measure that is relative to the mean and without a scale. The variable $t$ denotes the t-value and should be checked against the critical value of Student's t-distribution, with $2N - 2$ degrees of freedom.

Under the assumption that the data points in the windows are fully independent and Gaussian distributed one may use the delta method (Oehlert, 1992) to approximate the standard deviation of the log-transformed rms values in the signal and noise window ($\sigma_{RMS_{\log}}$).

The delta method offers the possibility to calculate the variance of a function of a random variable $X$:

$$Var[f(X)] \approx (f'(E[X]))^2 \cdot Var[X], \tag{14}$$

where $X$ denotes the random variable and $Var[X]$ and $E[X]$ the variance and expected value of X. Calculating the log-transformed rms value of a series of gaussian distributed random variables with mean 0 and unit variance is equivalent to:

$$RMS_{\log}(\chi^2(k)) = \log \sqrt{\frac{1}{k}\chi^2(k)}, \tag{15}$$

where $\chi^2(k)$ is chi-square distributed with k degrees of freedom. Applying the delta method (Eq. (14)) on that function enables to derive the standard deviation of the log-transformed rms-value $\sigma_{RMS_{\log}}$:

$$\sigma_{RMS_{\log}} = \sqrt{\frac{1}{2k}}, \tag{16}$$

where $k$ is the number of data points in both the signal and noise window. Since these window-lengths are tailored to the length of the signal to be observed, $k$ can alternatively be described as the length of the signal in data points. With this approximation and formula (12) Eq. (13) can be simplified to:

$$t \leqslant 0.5 \log(SNR_S^2 + 1)\sqrt{kN}. \tag{17}$$

Power values and the required sample size to reach a desired statistical power can now be calculated with standard techniques such as presented in Lehr (1992):

$$1 - \beta = cdf\left(0.5 \log(SNR_S^2 + 1) \cdot \sqrt{kN} - ppf\left(1 - \frac{\alpha}{2}\right)\right), \quad \text{or} \tag{18}$$

$$1 - \beta = cdf\left(0.5 \log(SNR_S^2 + 1) \cdot \frac{\sqrt{N/2}}{\sigma_{RMS_{\log}}} - ppf\left(1 - \frac{\alpha}{2}\right)\right) \tag{19}$$

where $\beta$ is the probability of making a type II error, $(1 - \beta)$ is the statistical power of the test and $\alpha$ is the significance level. $cdf()$ and $ppf()$ denote the cumulative distribution function and percent point function (inverse of the cdf of the standard normal distribution).

An inaccurateness of the approximation in formula (18) derives from the variable $k$–the length of the signal in data points. $k$ could easily be increased by increasing the sampling frequency of the analog-to-digital conversion. However, formula (18) assumes that the data points in the respective window are independent of each other. Oversampling the data will create an increased autocorrelation and therefore undermine this assumption. In that case the approximated $\sigma_{RMS_{\log}}$ would be too high. Hence, if using this approximation, the window length should be calculated with a surrogate sampling frequency of Nyquist rate relative to the bandwidth of the applied band-pass filter.

## References


Alegre M, Urriza J, Valencia M, Muruzabal J, Iriarte J, Artieda J. High-frequency oscillations in the somatosensory evoked potentials of patients with cortical myoclonus: pathophysiologic implications. J Clin Neurophysiol 2006;23:265–72.

Baker SN, Curio G, Lemon RN. EEG oscillations at 600 Hz are macroscopic markers for cortical spike bursts. J Physiol 2003;550:529–34.

Barth DS. Submillisecond synchronization of fast electrical oscillations in neocortex. J Neurosci 2003;23:2502–10.

Benjamini Y, Hochberg Y. Controlling the false discovery rate–a practical and powerful approach to multiple testing. J R Stat Soc Series B: Stat Methodol 1995;57:289–300.

Cracco RQ, Cracco JB. Somatosensory evoked potential in man: far field potentials. Electroencephalogr Clin Neurophysiol 1976;41:460–6.

Curio G. Ultrafast EEG activities. In: Niedermeyer E, da Silva FL, editors. Electroencephalography: Basic principles, clinical applications, and related fields. Baltimore: Lippincott Williams & Wilkins; 2004. p. 495–504.

Curio G, Mackert BM, Burghoff M, Koetitz R, Abraham-Fuchs K, Härer W. Localization of evoked neuromagnetic 600 Hz activity in the cerebral somatosensory system. Electroencephalogr Clin Neurophysiol 1994;91:483–7.

Gobbelé R, Waberski TD, Kuelkens S, Sturm W, Curio G, Buchner H. Thalamic and cortical high-frequency (600 Hz) somatosensory-evoked potential (SEP) components are modulated by slight arousal changes in awake subjects. Exp Brain Res 2000;133:506–13.

Hashimoto I. High-frequency oscillations of somatosensory evoked potentials and fields. J Clin Neurophysiol 2000;17:309–20.

Hashimoto I, Mashiko T, Imada T. Somatic evoked high-frequency magnetic oscillations reflect activity of inhibitory interneurons in the human somatosensory cortex. Electroencephalogr Clin Neurophysiol 1996;100:189–203.

Haueisen J, Heuer T, Nowak H, Liepert J, Weiller C, Okada Y, et al. The influence of lorazepam on somatosensory-evoked fast frequency (600 Hz) activity in MEG. Brain Res 2000;874:10–4.

Jansen BH, Agarwal G, Hegde A, Boutros NN. Phase synchronization of the ongoing EEG and auditory EP generation. Clin Neurophysiol 2003;114:79–85.

Kayser J, Tenke CE. Principal components analysis of Laplacian waveforms as a generic method for identifying ERP generator patterns: I. Evaluation with auditory oddball tasks. Clin Neurophysiol 2006;117:348–68.

Klostermann F, Funk T, Vesper J, Siedenberg R, Curio G. Double-pulse stimulation dissociates intrathalamic and cortical high-frequency (>400 Hz) SEP components in man. Neuroreport 2000a;11:1295–9.

Klostermann F, Funk T, Vesper J, Siedenberg R, Curio G. Propofol narcosis dissociates human intrathalamic and cortical high-frequency (> 400 Hz) SEP components. Neuroreport 2000b;11:2607–10.

Klostermann F, Nolte G, Curio G. Multiple generators of 600 Hz wavelets in human SEP unmasked by varying stimulus rates. Neuroreport 1999;10:1625–9.

Klostermann F, Nolte G, Losch F, Curio G. Differential recruitment of high frequency wavelets (600 Hz) and primary cortical response (N20) in human median nerve somatosensory evoked potentials. Neurosci Lett 1998;256:101–4.

Lehr R. Sixteen S-squared over D-squared: a relation for crude sample size estimates. Stat Med 1992;11:1099–102.

McCubbin J, Yee T, Vrba J, Robinson SE, Murphy P, Eswaran H, et al. Bootstrap significance of low SNR evoked response. J Neurosci Methods 2008;168:265–72.

Mochizuki H, Ugawa Y, Machii K, Terao Y, Hanajima R, Furubayashi T, et al. Somatosensory evoked high-frequency oscillation in Parkinson's disease and myoclonus epilepsy. Clin Neurophysiol 1999;110:185–91.

Nakano S, Hashimoto I. High-frequency oscillations in human somatosensory evoked potentials are enhanced in school children. Neurosci Lett 2000;291:113–6.
Nikulin VV, Linkenkaer-Hansen K, Nolte G, Lemm S, Müller KR, Ilmoniemi RJ, et al. A novel mechanism for evoked responses in the human brain. Eur J Neurosci 2007;25:3146–54.
Oehlert GW. A note on the delta method. Am Stat 1992;46:27–9.
Okada YC, Wu J, Kyuhou S. Genesis of MEG signals in a mammalian CNS structure. Electroencephalogr Clin Neurophysiol 1997;103:474–85.
Perrin F, Bertrand O, Pernier J. Scalp current density mapping: value and estimation from potential data. IEEE Trans Biomed Eng 1987;34:283–8.
Perrin F, Pernier J, Bertrand O, Echallier JF. Spherical splines for scalp potential and current density mapping. Electroencephalogr Clin Neurophysiol 1989;72:184–7.
Perrin F, Pernier J, Bertrand O, Echallier JF. Corrigenda to Spherical splines for scalp potential and current density mapping. Electroencephalogr Clin Neurophysiol 1990;76:565–6.
Rizzuto DS, Madsen JR, Bromfield EB, Schulze-Bonhage A, Seelig D, Aschenbrenner-Scheibe R, et al. Reset of human neocortical oscillations during a working memory task. Proc Natl Acad Sci USA 2003;100:7931–6.
Sachs L, Hedderich J. Angewandte Statistik Methodensammlung mit R. 12th ed. Berlin: Springer; 2006.
Sauseng P, Klimesch W, Gruber WR, Hanslmayr S, Freunberger R, Doppelmayr M. Are event-related potential components generated by phase resetting of brain oscillations? A critical discussion. Neuroscience 2007;146:1435–44.
Scheer HJ, Fedele T, Curio G, Burghoff M. Extension of non-invasive EEG into the kHz range for evoked thalamocortical activity by means of very low noise amplifiers. Physiol Meas 2011;32:N73–9.
Scheer HJ, Sander T, Trahms L. The influence of amplifier, interface and biological noise on signal quality in high-resolution EEG recordings. Physiol Meas 2006;27:109–17.
Shah AS, Bressler SL, Knuth KH, Ding M, Mehta AD, Ulbert I, et al. Neural dynamics and the fundamental mechanisms of event-related brain potentials. Cereb Cortex 2004;14:476–83.
Stockwell RG, Mansinha L, Lowe RP. Localization of the complex spectrum: The S transform. IEEE Trans Signal Process 1996;44:998–1001.
Telenczuk B, Nikulin VV, Curio G. Role of neuronal synchrony in the generation of evoked EEG/MEG responses. J Neurophysiol 2010;104:3557–67.
Urasaki E, Genmoto T, Yokota A, Maeda R, Akamatsu N. Effects of general anesthesia on high-frequency oscillations in somatosensory evoked potentials. J Clin Neurophysiol 2006;23:426–30.
Valencia M, Alegre M, Iriarte J, Artieda J. High frequency oscillations in the somatosensory evoked potentials (SSEP's) are mainly due to phase-resetting phenomena. J Neurosci Methods 2006;154:142–8.
Yamada T, Kameyama S, Fuchigami Y, Nakazumi Y, Dickins QS, Kimura J. Changes of short latency somatosensory evoked potential in sleep. Electroencephalogr Clin Neurophysiol 1988;70:126–36.